

Tracing the evolutionary stage of Bok globules: CCS and NH₃[★]

C. Marka¹, K. Schreyer¹, R. Launhardt², D. A. Semenov², and Th. Henning²

¹ Astrophysikalisches Institut und Universitätssternwarte (AIU), Schillergäßchen 2-3, D-07745 Jena, Germany

² Max-Planck-Institut für Astronomie (MPIA), Königstuhl 17, D-69117 Heidelberg, Germany

Received / Accepted

ABSTRACT

Aims. This work pursues the investigation of a previously proposed correlation between chemical properties and physical evolutionary stage of isolated low-mass star-forming regions. In the past, the $N_{\text{NH}_3}/N_{\text{CCS}}$ abundance ratio was suggested to be a potentially useful indicator for the evolutionary stage of cloud cores. We aim to study its applicability for isolated Bok globules.

Methods. A sample of 42 Bok globules with and without signs of current star formation was searched for CCS(2₁–1₀) emission, the observations were complemented with NH₃ measurements available in the literature and own observations. The abundance ratio of both molecules is discussed with respect to the evolutionary stage of the objects and in the context of chemical models.

Results. The $N_{\text{NH}_3}/N_{\text{CCS}}$ ratio could be assessed for 18 Bok globules and is found to be moderately high and roughly similar across all evolutionary stages from starless and prestellar cores towards internally heated cores harbouring protostars of Class 0, Class I or later. Bok globules with extremely high CCS abundance analogous to carbon-chain producing regions in dark cloud cores are not found. The observed range of $N_{\text{NH}_3}/N_{\text{CCS}}$ hints towards a relatively evolved chemical state of all observed Bok globules.

Key words. ISM: clouds – stars: formation – ISM: molecules – radio lines: ISM

1. Introduction

Bok globules, named in honor of the astronomer Bart Bok who drew attention to those objects and their possible role in the star formation process (Bok & Reilly 1947), appear as small and isolated dark clouds. Although the majority of stars in the Galaxy is formed in Giant Molecular Cloud complexes, the small globules have been recognized as particularly interesting targets for a study of low-mass star formation, since they represent a less complex environment and are therefore more easily described by theoretical models. The conditions inside Bok globules and the properties of the young stellar objects (YSOs) embedded therein have been studied at various wavelengths in several surveys in the past. Thermal radio emission arising from dust is observed at centimeter (Moreira et al. 1997, 1999) and millimeter wavelengths (Launhardt & Henning 1997, hereafter LH97; Henning & Launhardt 1998); submillimeter emission gives hints for deeply embedded protostars (Huard et al. 1999). With near-infrared observations, candidates for YSOs are identified and examined (Yun & Clemens 1995; Alves & Yun 1994; Racca et al. 2009). Molecular line observations provide information about the physical conditions, e.g. temperature, density, and magnetic fields, and trace the velocity structure of the clouds. They can be used to identify collapsing clouds (Wang et al. 1995) and reveal the presence of powerful molecular outflows (Yun & Clemens 1992, 1994b). A comprehensive overview of star formation in different stages is achieved by multi-wavelength studies (Launhardt et al. 2010, hereafter L2010).

In globules and cloud cores a large variety of molecules has been identified. The complex chemical processes leading to their formation and destruction are ruled by the local conditions, including surface reactions on ice-covered grains in the coldest and densest parts of the cloud, and are influenced by the heating of a forming star within the core or the ionizing interstellar radiation close to the cloud surface (review by, e.g., van Dishoeck & Blake 1998). While ammonia was the first polyatomic molecule to be discovered in the interstellar medium (review e.g. by Ho & Townes 1983), the CCS radical has been identified only two decades ago (Saito et al. 1987) and the main pathways leading to its formation are still under discussion (Suzuki et al. 1992; Petrie 1996; Sakai et al. 2007), although it is frequently observed along with other carbon-chain molecules (e.g., Hirota et al. 2009).

From a study of CCS and NH₃ among other molecules, Suzuki et al. (1992) found that carbon-chain molecules are abundant in the early evolutionary phases of dark cloud cores, while ammonia tends to be more abundant in more evolved, actively star-forming regions. This result was also supported by their chemical model calculations, where CCS is formed but also destroyed rapidly, while in turn a replenishment of the molecule is impeded by the increasing lock-up of carbon atoms in CO. In contrast, NH₃ forms in a sequence of very slow reactions and reaches its highest abundance in the late evolutionary phases. Therefore they proposed the $N_{\text{NH}_3}/N_{\text{CCS}}$ abundance ratio to be a possibly useful indicator for the evolutionary stage of star-forming clouds. In the following years, the abundance of both molecules in a number of Bok globules and around Herbig Ae/Be stars (Scappini & Codella 1996), as well as in a larger sample of intermediate-mass and low-mass star-forming regions with H₂O maser emission (de Gregorio-Monsalvo et al. 2006, hereafter dGM06) was examined. However, both studies suffered from a small number of CCS detections, which hindered a definitive judgement about this hypothesis. Focusing on statistics on a

[★] Based on observations obtained with the 100-m telescope of the MPIfR (Max-Planck-Institut für Radioastronomie) at Effelsberg and the 64-m Parkes radio telescope. The Parkes radio telescope is part of the Australia Telescope National Facility which is funded by the Commonwealth of Australia for operation as a National Facility managed by CSIRO.

Table 1. Overview of the observed globules.

| Object | RA (B1950) (h m s) | Dec (B1950) (° ' ") | Associated IRAS Source | Distance (Ref.) [pc] |
|-----------|--------------------------|---------------------------|---------------------------|----------------------------|
| CB 3 | 00 25 59.0 | +56 25 32 | 00259+5625 | 2500 (2) |
| CB 6 | 00 46 34.4 | +50 28 25 | 00465+5028 | 600 (3) |
| CB 12 | 01 35 24.3 | +64 47 59 | 01354+6447 | 800 (2) |
| CB 17 | 04 00 32.9 | +56 47 52 | (04005+5647) | 250 (3) |
| CB 22 | 04 37 23.5 | +29 49 17 | ... | 140 (2) |
| CB 23 | 04 40 20.5 | +29 33 26 | ... | 140 (2) |
| CB 26 | 04 55 56.1 | +52 00 17 | 04559+5200 | 140 (3) |
| CB 28 | 05 03 51.3 | -04 00 18 | 05038-0400 | 450 (3) |
| CB 34 | 05 44 05.7 | +20 59 30 | 05440+2059 | 1500 (3) |
| CB 44 | 06 04 43.0 | +19 28 19 | (06047+1923) | 700 (3) |
| CB 68 | 16 54 27.2 | -16 04 48 | 16544-1604 | 160 (3) |
| CB 125 | 18 12 39.0 | -18 12 14 | (18121-1813) | 200 (2) |
| CB 179 | 19 01 57.0 | -05 25 35 | (19018-0525) | 200 (2) |
| CB 188 | 19 17 54.0 | +11 30 10 | 19179+1129 | 300 (3) |
| CB 222 | 20 32 49.9 | +63 52 00 | 20328+6351 | 400 (3) |
| CB 224 | 20 35 30.9 | +63 42 48 | 20355+6343 | 400 (3) |
| CB 230 | 21 16 50.8 | +68 04 52 | 21169+6804 | 400 (3) |
| CB 232 | 21 35 14.4 | +43 07 17 | 21352+4307 | 600 (3) |
| CB 243 | 23 22 51.9 | +63 20 11 | 23228+6320 | 700 (3) |
| CB 244 | 23 23 48.9 | +74 01 10 | 23238+7401 | 200 (3) |
| CB 246 | 23 54 12.0 | +58 17 27 | ... | 140 (3) |
| BHR 12 | 08 07 39.0 | -35 55 54 | 08076-3556 | 400 (1) |
| BHR 13 | 08 26 44.1 | -33 36 31 | 08267-3336 | 400 (1) |
| BHR 15 | 07 14 27.5 | -43 52 26 | 07144-4352 | 400 (1) |
| BHR 23-1 | 08 33 42.6 | -40 28 02 | 08337-4028 | 500 (1) |
| BHR 28 | 07 26 20.0 | -50 58 18 | ... | 400 (1) |
| BHR 34 | 08 25 03.4 | -50 30 34 | 08250-5030 | 200 (3) |
| BHR 36 | 08 24 15.9 | -50 50 44 | 08242-5050 | 400 (1) |
| BHR 41 | 08 26 11.5 | -51 00 39 | 08261-5100 | 400 (1) |
| BHR 55 | 09 44 57.0 | -50 52 06 | 09449-5052 | 300 (1) |
| BHR 59 | 11 05 03.0 | -61 49 36 | ... | 200 (4) |
| BHR 71 | 11 59 03.1 | -64 52 11 | 11590-6452 | 200 (3) |
| BHR 74 | 12 19 21.0 | -66 10 30 | ... | 175 (4) |
| BHR 86 | 13 03 41.4 | -76 44 03 | 13036-7644 | 180 (3) |
| BHR 111 | 15 38 34.0 | -52 38 21 | ... | 250 (4) |
| BHR 121-1 | 16 54 59.6 | -50 30 58 | 16549-5030 | 125 (4) |
| BHR 121-2 | 16 55 27.8 | -50 31 01 | 16554-5031 | 125 (4) |
| BHR 137 | 17 18 08.6 | -44 06 17 | (17181-4405) | 700 (3) |
| BHR 138 | 17 15 54.0 | -43 24 04 | 17159-4324 | 225 (4) |
| BHR 139-1 | 17 17 15.9 | -43 16 54 | 17172-4316 | 225 (4) |
| BHR 140-1 | 17 19 18.8 | -43 19 24 | 17193-4319 | 225 (4) |
| BHR 148 | 17 01 09.2 | -36 13 59 | 17011-3613 | 175 (4) |

References. (1) Bourke et al. (1995b); (2) Launhardt & Henning (1997); (3) Launhardt et al. (2010) and private communication; (4) Racca et al. (2009).

large number of dense cores within the Perseus Molecular cloud, a recent work by Foster et al. (2009) provided evidence for a lower fractional abundance of CCS in protostellar cores compared to starless cores.

In this work we are focusing on small Bok globules, typically forming only single or few low-mass stars, since they represent the most secluded star-forming environments available for investigation. An interference by other nearby, possibly high-mass, forming stars can be excluded. Moreover, a mixing with ambient material which could modify the chemical composition and exacerbate a comparison with theoretical models, as it is possible in the case of a dense core inside a larger cloud complex, is implausible for the isolated globules. An overview of the sample examined in this work is given in Sect. 2, followed by a description of the observational results and analysis in Sect. 4.

The discussion of the derived physical parameters is presented in Sect. 5, concluding remarks are given in Sect. 6.

2. Description of the sample

Our sample consists of 42 Bok globules from the catalogs of Clemens & Barvainis (1988) for the northern hemisphere and Bourke et al. (1995a) for the southern globules. The northern sources have been searched for NH₃(1,1) and (2,2) emission with the Effelsberg 100-m telescope in the survey of Lemme et al. (1996, hereafter L96), while the southern globules are included in the NH₃ survey of Bourke et al. (1995b, hereafter BHR95b), so that a uniform set of ammonia measurements is available for comparison with our data. Table 1 lists the positions of the CCS measurement, the IRAS point sources associated with the globules (sources in brackets were located outside the telescope beam), and their distance. Following the classification scheme of L2010, we sorted the objects into three groups according to the presence and evolutionary class (cf. Lada 1987; André et al. 1993) of embedded YSOs:

- Group –I: Starless or prestellar globules, or only very young and very low-luminosity source embedded.
- Group 0: Globules harbouring a Class 0 protostar.
- Group I: Globules containing YSOs of Class I or later.

The classification of the individual clouds is indicated in Table 2. Where too sparse observations of the specific globule prevent a reliable identification of the evolutionary group, a presumptive classification is given in brackets. It should be emphasized that especially prestellar cores or Class 0 protostars will most probably remain unidentified when there is a lack of detailed maps of molecular emission and/or millimeter continuum emission. A detailed discussion for most globules of the sample can be found in L2010 and the references therein, while a number of southern globules has been classified in Racca et al. (2009). In the following we comment therefore only shortly on the globules not described there.

CB 3. A compact submillimeter source without infrared counterpart is located at the center of a bipolar molecular outflow (Yun & Clemens 1994b) and was suggested to consist of an aggregate of Class 0 sources by Huard et al. (2000). The source IRAS 00259+5625 is located 15'' away, its near-infrared counterpart was classified as Class II object (Yun & Clemens 1994a, 1995). The globule also harbours a H₂O-maser (Scappini et al. 1991,dGM06); it is believed to be rather an evolved intermediate to high-mass star-forming region (Launhardt et al. 1998b; Codella & Bachiller 1999).

CB 12. An associated IRAS point source is detected at 60 and 100 μ m, but neither a molecular outflow (Yun & Clemens 1992) nor dust continuum emission at 1.3 mm (LH97) point towards the presence of an embedded protostar.

CB 22 and CB 23. Both globules are not detected in the far-infrared (no IRAS sources) or in the 1.3 mm dust continuum (LH97). According to the shape of spectral lines, CB 22 seems to be quiescent while CB 23 shows signatures of a possible infall motion (Lee et al. 1999, 2004).

CB 28. Only emission longward of 60 μ m was detected by IRAS towards this globule; searches for outflows (Yun & Clemens 1994b) and YSO candidates in the near-infrared (Yun & Clemens 1994a) resulted in no detections.

CB 34. Numerous studies suggest multiple star formation in the globule. Five submillimeter sources were detected by

Huard et al. (2000) and classified as probable Class 0 objects. The aggregate of protostars is associated with a system of multiple outflows (Codella & Scappini 2003) and jets (Moreira & Yun 1995). Evidence for the presence of more evolved Class I and Class II objects is provided by the detection of several very red objects in the near-infrared (Alves & Yun 1995).

CB 44. The associated IRAS source cited by Clemens & Barvainis (1988) resides at the very edge of the globule. Two 3.6 cm continuum sources without infrared counterparts, candidate Class 0 objects, were detected by Moreira et al. (1999) but no detection was possible at shorter wavelengths (e.g. at 1.3 mm by LH97).

CB 125. Several IRAS point sources are located in the vicinity, but none within the area of highest extinction visible on optical images of the globule. Both IRAS 18127-1803 and IRAS 18122-1818 have reliable fluxes only at 12 and 25 μm , they were considered as candidate pre-main sequence star (LH97) and YSO (Lee & Myers 1999), respectively. The 100 μm detection towards IRAS 18130-1824 was considered as cirrus emission due to the lack of submillimeter continuum emission (Huard et al. 1999). Line observations in CS towards IRAS 18126-1820 at the southern edge of CB 125 show unsuspicious gaussian line profiles (Launhardt et al. 1998a). Due to the presence of candidate YSOs close to the cloud, we assume an evolved stage.

CB 179. The association with a cold infrared source detected only at 60 and 100 μm , the absence of 1.3 mm continuum emission (LH97) and narrow, weak CO lines (Clemens et al. 1991) suggest an early evolutionary stage.

CB 222. Neither is the associated IRAS source detected at wavelengths shortward of 60 μm , nor is 1.3 mm dust emission found towards this globule (LH97). Together with unsuspicious gaussian line profiles measured in CS (Launhardt et al. 1998a), we assume an early evolutionary stage for CB 222.

BHR 13. The narrow CO line profiles observed towards this cometary globule are supposed to arise from cold, quiescent gas (Otrupcek et al. 2000), while the associated IRAS source was identified as a T Tauri star (Sahu & Sahu 1992).

BHR 15. The IRAS source associated with this cometary globule is detected only at 60 and 100 μm , and CO line profiles typical of cold, quiescent gas have been observed (Otrupcek et al. 2000). Therefore, an early evolutionary stage is assumed.

BHR 23. Santos et al. (1998) conclude from near-infrared observations that an aggregate of several YSOs might be harboured by this globule. High-velocity wings in CO lines detected by Urquhart et al. (2009) and Otrupcek et al. (2000) might indicate the presence of a molecular outflow. Methanol maser emission, which is believed to be associated with high-mass star formation, was also observed towards this source (Walsh et al. 1997).

BHR 28, BHR 59, BHR 74 and BHR 111. These globules do not harbour any IRAS sources. Profiles of CO lines observed towards BHR 74 and the cometary globule BHR 28 suggest the presence of cold and quiescent gas (Otrupcek et al. 2000). In BHR 59 and BHR 111 the detection of line wings might indicate the presence of several blended velocity components or outflow motions (Otrupcek et al. 2000). However, no more detailed observations are available for those globules.

BHR 41. Santos et al. (1998) classified the two near-infrared sources separated by 4'' seen at the position of the IRAS source as likely Class I objects. However, no 1.3 mm dust emission was detected towards this source (L2010).

BHR 137. Santos et al. (1998) detected three infrared sources at the IRAS position, two of which are likely Class II objects. However, the IRAS source is located at the rim of the globule and it is unsure if it is related. Emission in the 1.3 mm dust continuum has been detected by Henning & Launhardt (1998), as well as a blue wing in the CO emission. L2010 suggested a rather early evolutionary stage.

Some of the globules are known to contain multiple sources in different evolutionary stages, namely CB 3 (Yun & Clemens 1994a; Huard et al. 2000), CB 34, CB 224, CB 232, CB 243, CB 244 and BHR 12 (L2010). In such cases, where there are sources of different evolutionary stage within the beam of the NH₃ and CCS observations, we assigned the globule to the evolutionary group that agrees with the source from which most of the mm dust emission arises, i.e., which has the largest reservoir of cold gas and is therefore dominating the detected line emission. However, it cannot be excluded that one of the other sources also contributes to the detected line emission. Also, the maturity of individual globules might be underestimated, because the presence of an evolved YSO nearby a pre/protostellar core possibly affects its chemistry, especially since in most cases the projected separation between the differently evolved sources is only a few thousand AU. We have noted these cases in Table 2.

3. Observations

Observations in CCS(2₁–1₀) of all objects from the Clemens & Barvainis (1988) catalog listed in Table 1, as well as NH₃(1,1) and (2,2) observations for three globules, have been carried out with the Effelsberg 100-m telescope of the Max-Planck-Institut für Radioastronomie (MPIfR) during March 14 and 15, 1999. A maser receiver in the primary focus was used with a 1024 channel autocorrelator. The system temperature was in the range of 80 and 110 K. For the CCS(2₁–1₀) line at 22.344 GHz the total bandwidth of 6.25 MHz of the spectrometer was used, providing a velocity resolution of 0.08 km s^{−1}. The autocorrelator was split into 2×512 channels for the observations of the NH₃(1,1) and (2,2) lines at 23.694 GHz and 23.722 GHz, respectively, corresponding to a velocity resolution of 0.15 km s^{−1}. At the used frequencies, the beam diameter (FWHP) was 40''. Frequency switching was used with a total integration time per source of 30–60 min for the CCS line and 5–30 min for the NH₃ lines. The pointing was checked every 2 hours by cross-scans on nearby quasars. Typically, the pointing accuracy was better than 5'' at similar elevations. The focus was checked on strong continuum sources at the beginning of the observing run and after sunset and sunrise. The data were calibrated using cross scans on continuum sources with known flux density (Ott et al. 1994). As a primary calibrator, NGC 7027 was used. The antenna temperatures were converted to a main beam brightness temperature T_{mb} by correcting with the elevation dependent gain, the beam and aperture efficiency. The calibration is estimated to be accurate within ~15%.

The 21 sources from the catalog of Bourke et al. (1995a) have been observed with the Parkes 64m telescope during March 2010 in the CCS(2₁–1₀) transition, and ten of them additionally in NH₃(1,1) – namely those sources, where the core or YSO of interest was not included in the beam of BHR95b. The 13MM receiver and a digital filterbank with a bandwidth of 8 MHz and 2048 channels were employed, resulting in a velocity resolution of 0.05 km s^{−1}. The beam diameter was 1' and the pointing was estimated to be accurate within 20''. Except of BHR 15, BHR 23

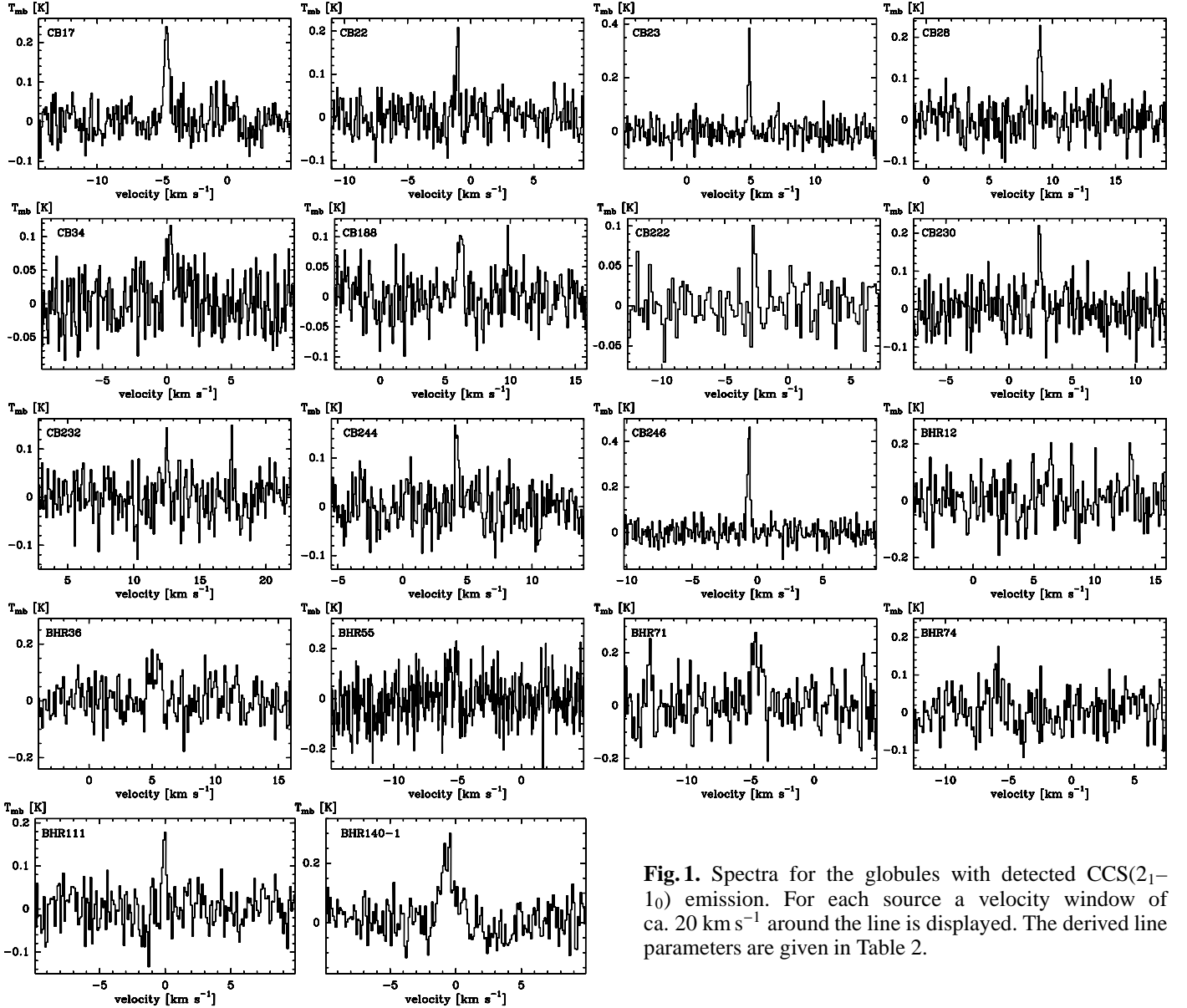


Fig. 1. Spectra for the globules with detected CCS(2_1-1_0) emission. For each source a velocity window of ca. 20 km s⁻¹ around the line is displayed. The derived line parameters are given in Table 2.

and BHR 28 which were observed in the position switching mode, frequency switching with a throw of 1 MHz for the CCS and 0.3 MHz for the NH₃ line, respectively, was used with integration times of 20–60 min. Typical system temperatures ranged from 70 to 130 K. After correction of the elevation-dependent gain, we applied relative calibration by means of repeated observations of BHR 71 compared to the measurements of BHR95b. Hereby, it is ensured that the scale of our measurements and those of BHR95b, to be used for calculation of the $N_{\text{NH}_3}/N_{\text{CCS}}$ ratio, match. Although with this approach the absolute accuracy of our calibration is expected to be not optimal, comparison of the CCS observations for CB 28, which have been carried out in Parkes and Effelsberg, show consistency.

The spectra for all globules showing (possible) detections in the CCS line are displayed in Fig. 1.

4. Results

The results of the observations are summarized in Tables 2 and 3. Out of the 42 globules observed, thirteen were detected in the CCS(2_1-1_0) line with a signal-to-noise ratio of at least three.

Additional five globules show emission at a slightly lower significance level, but we believe them to be real detections since their LSR velocities are in agreement with those of ammonia lines observed by BHR95b. In contrast, NH₃(1,1) remained undetected only towards three globules of our sample.

From the further discussion we exclude CB 3, CB 34 and BHR 23 because they likely contain clusters or high-mass star-forming regions, as well as BHR 13, BHR 59 and BHR 111 because of their very uncertain evolutionary stage, and BHR 12 because of the presence of two equally massive sources in different evolutionary groups (the source is however included in Figs. 2 and 6). Considering only the globules with fairly reliable evolutionary group (i.e. group given without brackets in Table 2), CCS emission is present in 70% (seven out of ten objects) of the globules belonging to the starless or prestellar globules of group –I, in 40% of the objects of group 0 (clouds containing Class 0 protostars; four detections) and 33% of the group I objects (YSOs of Class I or later embedded; three out of nine detected). The overall detection rate (43%) of CCS(2_1-1_0) in our sample is therefore larger than found in some earlier studies of low-mass star-forming regions, globules and dark clouds (about 18–33% in the

Table 2. Derived CCS(2₁–1₀) line parameters and column densities for CCS and ammonia, and resulting abundance ratio $N_{\text{NH}_3}/N_{\text{CCS}}$.

| Source | Group | ν_{LSR} [km s ⁻¹] | T_{mb} [mK] | $\Delta\nu_{\text{obs}}$ [km s ⁻¹] | $\int T_{\text{mb}} d\nu$ [mK km s ⁻¹] | $\Delta\nu_{\text{nth}}$ [km s ⁻¹] | N_{CCS} [10 ¹² cm ⁻²] | N_{NH_3} (Ref.) [10 ¹⁴ cm ⁻²] | $N_{\text{NH}_3}/N_{\text{CCS}}$ |
|-----------|------------------|---|-------------------------|---|---|---|--|--|----------------------------------|
| CB 3 | 0 | ... | < 96 | ... | ... | ... | < 1.42 | 1.54 ± 0.26* (1) | > 104 |
| CB 6 | I | ... | < 90 | ... | ... | ... | < 1.32 | 0.29 ± 0.07* | > 22 |
| CB 12 | -I | ... | < 117 | ... | ... | ... | < 1.70 | 1.45 ± 0.24* (1) | > 86 |
| CB 17 | -I ^a | -4.65 ± 0.02 | 233 ± 37 | 0.45 ± 0.06 | 112 ± 12 | 0.44 ± 0.06 | 4.89 ± 0.53 | 13.84 ± 3.74 | 201 ± 47 |
| CB 22 | -I | -1.03 ± 0.01 | 233 ± 37 | 0.15 ± 0.05 | 36 ± 7 | 0.08 ± 0.08 | 1.42 ± 0.29 | 3.64 ± 0.87 (1) | 257 ± 80 |
| CB 23 | -I | 4.86 ± 0.01 | 375 ± 39 | 0.17 ± 0.02 | 66 ± 8 | 0.11 ± 0.03 | 2.39 ± 0.28 | 10.1 ± 1.1 (1) | 422 ± 67 |
| CB 26 | I | ... | < 114 | ... | ... | ... | < 1.67 | 0.48 ± 0.18* (1) | > 28 |
| CB 28 | -I | 9.01 ± 0.02 | 223 ± 40 | 0.29 ± 0.04 | 69 ± 9 | 0.26 ± 0.05 | 3.48 ± 0.45 | 1.95 ± 1.18 (1) | 56 ± 34 |
| CB 34 | 0 | 0.17 ± 0.05 | 119 ± 37 | 0.60 ± 0.14 | 57 ± 10 | 0.59 ± 0.15 | 2.64 ± 0.53 | 0.92 ± 0.44* (1) | 34 ± 17 |
| CB 44 | (-I) | ... | < 132 | ... | ... | ... | < 1.95 | 0.65 ± 0.15* (1) | > 34 |
| CB 68 | 0 | ... | < 120 | ... | ... | ... | < 1.48 | 12.7 ± 0.9 (1) | > 860 |
| CB 125 | (I) | ... | < 132 | ... | ... | ... | < 1.88 | 6.01 ± 1.63 (1) | > 320 |
| CB 179 | -I | ... | < 102 | ... | ... | ... | < 1.49 | 0.59 ± 0.15* (1) | > 40 |
| CB 188 | I | 6.14 ± 0.04 | 111 ± 35 | 0.44 ± 0.08 | 52 ± 10 | 0.42 ± 0.09 | 2.21 ± 0.41 | 1.10 ± 0.33* (1) | 50 ± 17 |
| CB 222 | -I | -2.70 ± 0.05 | 102 ± 25 | 0.34 ± 0.12 | 36 ± 12 | 0.31 ± 0.14 | 1.54 ± 0.53 | 0.65 ± 0.08* | 42 ± 15 |
| CB 224 | 0 ^b | ... | < 144 | ... | ... | ... | < 2.61 | 6.23 ± 1.17 (1) | > 239 |
| CB 230 | I ^c | 2.41 ± 0.03 | 190 ± 49 | 0.33 ± 0.12 | 66 ± 16 | 0.30 ± 0.13 | 2.79 ± 0.66 | 0.71 ± 0.24* (1) | 26 ± 9 |
| CB 232 | -I ^d | 12.50 ± 0.03 | 138 ± 41 | 0.23 ± 0.07 | 34 ± 9 | 0.19 ± 0.09 | 1.42 ± 0.38 | 0.54 ± 0.21* (1) | 38 ± 15 |
| CB 243 | -I ^e | ... | < 114 | ... | ... | ... | < 1.67 | 2.77 ± 1.04 (1) | > 166 |
| CB 244 | 0 | 4.18 ± 0.03 | 162 ± 41 | 0.31 ± 0.07 | 54 ± 10 | 0.29 ± 0.07 | 1.96 ± 0.37 | 8.08 ± 2.37** (1) | 412 ± 143 |
| CB 246 | -I | -0.65 ± 0.01 | 462 ± 39 | 0.24 ± 0.03 | 120 ± 11 | 0.21 ± 0.03 | 5.67 ± 0.49 | 7.70 ± 1.01 (1) | 136 ± 18 |
| BHR 12 | I+0 ^f | 6.36 ± 0.07 | 190 ± 68 | 0.35 ± 0.15 | 71 ± 23 | 0.33 ± 0.16 | 2.75 ± 0.88 | 5.4 (2) | 196 ± 62 |
| BHR 13 | (I) | ... | < 294 | ... | ... | ... | < 7.14 | 0.68 ± 0.22* | > 10 |
| BHR 15 | (-I) | ... | < 221 | ... | ... | ... | < 5.40 | 0.7 (2) | > 13 |
| BHR 23 | (I) | ... | < 206 | ... | ... | ... | < 5.01 | 4.07 ± 0.67* (2) | > 81 |
| BHR 28 | (-I) | ... | < 209 | ... | ... | ... | < 5.08 | 3.2 (2) | > 63 |
| BHR 34 | 0 | ... | < 244 | ... | ... | ... | < 5.95 | 0.91 ± 0.50* | > 15 |
| BHR 36 | I | 5.23 ± 0.11 | 125 ± 61 | 0.94 ± 0.17 | 124 ± 26 | 0.93 ± 0.17 | 4.13 ± 0.86 | 7.22 ± 2.01 | 175 ± 60 |
| BHR 41 | I ^g | ... | < 198 | ... | ... | ... | < 5.07 | 1.02 ± 0.54* | > 20 |
| BHR 55 | 0 ^h | -5.36 ± 0.05 | 173 ± 93 | 0.27 ± 0.10 | 100 ± 62 | 0.25 ± 0.11 | 3.38 ± 2.11 | 5.30 ± 1.45 | 157 ± 107 |
| BHR 59 | (0) | ... | < 221 | ... | ... | ... | < 5.37 | 2.19 ± 0.32* (2) | > 41 |
| BHR 71 | 0 ⁱ | -4.52 ± 0.08 | 209 ± 78 | 0.87 ± 0.14 | 193 ± 33 | 0.86 ± 0.14 | 6.63 ± 1.15 | 12.25 ± 2.75 | 185 ± 51 |
| BHR 74 | (-I) | -5.89 ± 0.09 | 111 ± 45 | 0.52 ± 0.22 | 61 ± 18 | 0.50 ± 0.22 | 2.19 ± 0.66 | 1.3 (2) | 59 ± 18 |
| BHR 86 | 0 | ... | < 264 | ... | ... | ... | < 7.23 | 5.0 (2) | > 69 |
| BHR 111 | (0) | -0.07 ± 0.03 | 186 ± 44 | 0.30 ± 0.06 | 59 ± 12 | 0.28 ± 0.07 | 2.42 ± 0.48 | 3.6 (2) | 149 ± 29 |
| BHR 121-1 | I | ... | < 212 | ... | ... | ... | < 5.14 | 0.42 ± 0.23* | > 8 |
| BHR 121-2 | I | ... | < 201 | ... | ... | ... | < 4.90 | 0.48 ± 0.35* | > 10 |
| BHR 137 | (0) | ... | < 245 | ... | ... | ... | < 5.95 | 4.3 (2) | > 72 |
| BHR 138 | 0 | ... | < 223 | ... | ... | ... | < 5.41 | < 0.46* | ... |
| BHR 139-1 | I | ... | < 211 | ... | ... | ... | < 5.12 | < 0.45* | ... |
| BHR 140-1 | 0 | -0.63 ± 0.07 | 221 ± 55 | 1.21 ± 0.16 | 285 ± 31 | 1.21 ± 0.16 | 11.1 ± 1.20 | 20.4 (2) | 184 ± 20 |
| BHR 148 | 0 | ... | < 282 | ... | ... | ... | < 3.52 | < 0.80* | ... |

Notes. (*) Optical thin approximation used to derive N_{NH_3} , (**) N_{NH_3} derived from available map and map-averaged T_{rot} and T_{ex} , since NH₃ peak lies outside the CCS beam. ^(a) Main core is prestellar (SMM1+2), but there is a low-luminosity Class I source 20'' away, slightly outside the beam. ^(b) Main core is Class 0 (SMM1), but there is a Class I source 30'' away (not inside the telescope beam). ^(c) Contains two Class I IR sources 10'' apart. ^(d) Main core is most likely prestellar (SMM), but there is a Class I source 12'' away. ^(e) Main core is most likely prestellar (SMM1), but there is a Class I source 10'' away. ^(f) A Class 0 and Class I YSO with cores of similar mass separated by 20'' inside the beam. ^(g) Two close (4'' separation) infrared sources of Class I (Santos et al. 1998). ^(h) Two close lines with comparable width ≈ 0.27 km s⁻¹ in CCS. ⁽ⁱ⁾ Double protostellar core with two IR sources 17'' apart.

References. (1) Lemme et al. (1996); (2) Bourke et al. (1995b).

studies of Scappini & Codella 1996, dGM06, and Suzuki et al. 1992), and closer to the 50% detection rate of a survey of dense cores in the Perseus Molecular Cloud (Rosolowsky et al. 2008; Foster et al. 2009). For ammonia, strong emission in the sense that the hyperfine structure of the NH₃(1,1) transition is detected, is present in 80% of the objects from group -I, and in 70% and 22% of the objects of group 0 and I, respectively.

4.1. Analysis of CCS lines

In Table 2, Column (1) lists the object number from the Clemens & Barvainis (1988) or Bourke et al. (1995a) catalog, (2) the assigned evolutionary group (cf. Sect. 2), (3) the LSR-velocity, (4) the main beam brightness temperature, (5) the observed line width (FWHM) including instrumental broadening (of 0.08 km s⁻¹ and 0.05 km s⁻¹ for the CB and BHR sources, respectively), and in (6) the integrated intensity of the line. Column (7) contains the nonthermal linewidths, (8) the calculated total column densities for CCS, (9) the ammonia column

Table 3. Results of the NH₃(1,1) and NH₃(2,2) observations.

| Source | $\nu_{\text{LSR}(1,1)}$ [km s ⁻¹] | $T_{\text{mb}(1,1)}$ [K] | $\Delta\nu_{\text{obs}(1,1)}$ [km s ⁻¹] | $\nu_{\text{LSR}(2,2)}$ [km s ⁻¹] | $T_{\text{mb}(2,2)}$ [K] | $\Delta\nu_{\text{obs}(2,2)}$ [km s ⁻¹] | $\tau_{\text{m}(1,1)}$ [K] | T_{ex} [K] |
|-----------|--|-----------------------------|--|--|-----------------------------|--|-------------------------------|------------------------|
| CB 6 | -12.45 ± 0.09 | 0.15 ± 0.05 | 0.62 ± 0.18 | ... | < 0.14 | ... | ... | 6* |
| CB 17 | -4.65 ± 0.01 | 1.71 ± 0.10 | 0.34 ± 0.02 | -4.70 ± 0.06 | 0.17 ± 0.04 | 0.79 ± 0.18 | 2.8 ± 0.6 | 5.4 ± 0.4 |
| CB 222 | -2.71 ± 0.04 | 0.29 ± 0.05 | 0.72 ± 0.10 | ... | < 0.11 | ... | ... | 6* |
| BHR 13 | 6.44 ± 0.06 | 0.30 ± 0.07 | 1.25 ± 0.18 | ... | ... | ... | ... | 6* |
| BHR 34 | 4.78 ± 0.04 | 0.50 ± 0.10 | 0.69 ± 0.11 | ... | ... | ... | ... | 6* |
| BHR 36 | 5.27 ± 0.02 | 1.21 ± 0.07 | 0.52 ± 0.04 | ... | ... | ... | 1.9 ± 0.5 | 4.3 ± 0.2 |
| BHR 41 | 5.46 ± 0.05 | 0.36 ± 0.08 | 0.92 ± 0.16 | ... | ... | ... | ... | 6* |
| BHR 55 | -5.50 ± 0.01 | 1.45 ± 0.11 | 0.51 ± 0.04 | ... | ... | ... | 1.2 ± 0.3 | 5.1 ± 0.4 |
| BHR 71 | -4.39 ± 0.02 | 3.56 ± 0.11 | 0.71 ± 0.03 | ... | ... | ... | 1.5 ± 0.3 | 8.0 ± 0.6 |
| BHR 121-1 | -12.61 ± 0.04 | 0.26 ± 0.06 | 0.61 ± 0.08 | ... | ... | ... | ... | 6* |
| BHR 121-2 | -12.52 ± 0.05 | 0.27 ± 0.07 | 0.68 ± 0.15 | ... | ... | ... | ... | 6* |
| BHR 138 | ... | < 0.21 | ... | ... | ... | ... | ... | 6* |
| BHR 139-1 | ... | < 0.20 | ... | ... | ... | ... | ... | 6* |
| BHR 148 | ... | < 0.36 | ... | ... | ... | ... | ... | 6* |

Notes. (*) T_{ex} is adopted as average value from Lemme et al. (1996) and Bourke et al. (1995b).

densities from own observations or collected from the literature, and (10) the abundance ratio $N_{\text{NH}_3}/N_{\text{CCS}}$. Source velocity ν_{LSR} , linewidth $\Delta\nu_{\text{obs}}$, peak intensity T_{mb} and integrated intensity $\int T_{\text{mb}} d\nu$ were derived by Gaussian fits of the lines using CLASS¹. For the error of T_{mb} , the root mean square (rms) noise of the spectrum, and for the other quantities the standard deviations of the Gaussian fits to the lines are listed in Table 2. The average rms noise level of the obtained spectra is 38 mK for the CB sources and 72 mK for the BHR sources. As upper limits for the non-detections, a peak intensity of 3 rms is given. In the case of CB 34 and BHR 55 the observed CCS line was not well approximated by a Gaussian profile, therefore the value in Table 2 represents the intensity integrated under the actual line rather than under the fitted profile.

The total column densities N_{CCS} were calculated under the assumption of a local thermodynamic equilibrium (LTE):

$$N = \frac{8\pi\nu_{ij}^2 g_0}{c^2 g_j} \frac{Q(T_{\text{ex}})}{A_{ji}} \frac{e^{E_j/kT_{\text{ex}}}}{(e^{h\nu_{ij}/kT_{\text{ex}}} - 1)} \int \tau_\nu d\nu, \quad (1)$$

where ν_{ij} denotes the frequency of the transition, g_0 and g_j are the statistical weights of the ground state and of the upper rotational level, respectively, E_j is the energy of the upper level, $Q(T_{\text{ex}})$ denotes the partition function for an excitation temperature T_{ex} , A_{ji} is the Einstein coefficient for spontaneous emission and τ_ν the optical depth. We assumed the emission to be optically thin, thus the relation between optical depth and main beam brightness temperature T_{mb} from the radiative transfer equation is given by

$$\int \tau_\nu d\nu = \frac{k}{hc} \left(\frac{1}{e^{h\nu_{ij}/kT_{\text{ex}}} - 1} - \frac{1}{e^{h\nu_{ij}/kT_{\text{bg}}} - 1} \right)^{-1} \int T_{\text{mb}} d\nu, \quad (2)$$

where $T_{\text{bg}} = 2.73$ K is the cosmic background temperature. Since only one rotational transition of CCS was observed, the excitation temperature could not be determined. We adopted $T_{\text{ex}} \approx 5$ K, equal to the average value for a number of dark cloud cores as found by Suzuki et al. (1992). Restricting to the measured CCS(2₁-1₀) transition with $A_{2_1-1_0} = 4.33 \times 10^{-7}$ s⁻¹ and

$E_{2_1}/k = 1.61$ K (Wolkovitch et al. 1997), and $Q_{\text{ex}}(5 \text{ K}) = 23.80$ (Lai & Crutcher 2000), the column density ensues as follows:

$$N_{\text{CCS}} [\text{cm}^{-2}] = 2.92 \times 10^{13} \int T_{\text{mb}} d\nu [\text{K km s}^{-1}] \quad (3)$$

A 4 K higher excitation temperature would result in a moderate increase of about 40% for the column density. For the not detected lines the upper limit for $\int T_{\text{mb}} d\nu$ was estimated as $1.06 T_{\text{mb}} \overline{\Delta\nu}$, where $\overline{\Delta\nu}$ was taken to be the average of the detected line widths, 0.32 km s⁻¹ for the CB sources and 0.64 km s⁻¹ for the BHR sources.

4.2. Ammonia lines

For most of the sources in our sample, ammonia column densities were derived in the papers of L96 and BHR95b. For our own ammonia observations, column densities were derived as outlined in the following. If hyperfine structure for the NH₃(1,1) transition was sufficiently strong, a fit with the available procedure within the CLASS package was performed to obtain optical depth of the main line $\tau_{\text{m}(1,1)}$ and intrinsic linewidth $\Delta\nu_{\text{int}}$. Otherwise a Gaussian profile was fitted to the main line. The derived line parameters are summarized in Table 3, where $\Delta\nu_{\text{obs}(1,1)}$ refers to the intrinsic linewidth for CB 17, BHR 36, BHR 55 and BHR 71, and to the width of a single Gaussian fitted to the main component otherwise. Further analysis was performed following standard procedures and assumptions (e.g. Ungerechts et al. 1980; Stutzki 1984). The excitation temperature T_{ex} was calculated from

$$T_{\text{ex}} \approx \frac{T_{\text{mb}(1,1)}}{f_b (1 - e^{-\tau_{\text{m}(1,1)}})} + T_{\text{bg}}, \quad (4)$$

with the beam filling factor f_b and brightness temperature of the main line $T_{\text{mb}(1,1)}$. The column density in the (1,1) levels then follows as

$$N_{(1,1)} = \frac{4\pi^{3/2} \nu_{11}^3}{\sqrt{\ln 2} c^3} \frac{\Delta\nu_{\text{int}}}{A_{11}} \frac{\tau_{\text{m}(1,1)}}{s_m} \frac{1 + e^{-h\nu_{11}/kT_{\text{ex}}}}{1 - e^{-h\nu_{11}/kT_{\text{ex}}}}. \quad (5)$$

with the rate coefficient $A_{11} = 1.67 \times 10^{-7}$ s⁻¹ and frequency ν_{11} of the NH₃(1,1) transition; s_m denotes the line strength at the main component, the value of which depends on the intrinsic

¹ part of the program package GILDAS (Grenoble Image and Line Data Analysis Software), see <http://www.iram.fr/IRAMFR/GILDAS/>.

linewidth of the hyperfine components blended in the main line. The complete ammonia column density is then estimated by

$$N_{\text{NH}_3} = N_{(1,1)} \left(1 + \frac{1}{3} e^{\frac{22.7 \text{ K}}{T_{\text{rot}}}} + \frac{5}{3} e^{\frac{-41.2 \text{ K}}{T_{\text{rot}}}} + \frac{14}{3} e^{\frac{-100.3 \text{ K}}{T_{\text{rot}}}} \right). \quad (6)$$

Since we did not observe the NH₃(2,2) transition in most cases, we could derive the rotational temperature (see e.g. Ungerechts et al. 1980) only for CB 17 ($T_{\text{rot}} = 8.1 \pm 0.5 \text{ K}$). For the other sources we adopted a rotational temperature of 10 K for normal and 13 K for cometary globules (BHR 12, BHR 13, BHR 15, BHR 28), i.e. average values from the papers of L96 and BHR95b, for the calculation.

Where the hyperfine structure was weak or only the main line of the NH₃(1,1) transition was detectable, so that the optical depth could not be derived, the column densities were estimated in the optically thin approximation with

$$N_{(1,1)} = \frac{16\pi\nu_{11}^3}{c^3} \frac{k}{h\nu_{11}} \frac{1}{f_b A_{11}} \frac{1 + e^{h\nu_{11}/kT_{\text{ex}}}}{1 - \frac{e^{h\nu_{11}/kT_{\text{ex}}}-1}{e^{h\nu_{11}/kT_{\text{bg}}}-1}} \int T_{\text{mb}(1,1)} d\nu, \quad (7)$$

where $\int T_{\text{mb}(1,1)} d\nu$ is the intensity integrated over the main component of the NH₃(1,1) transition. For the excitation temperature in equation 7, the average value found by L96 and BHR95b, $T_{\text{ex}} = 6 \text{ K}$ has been assumed. The total column density can then be calculated from equation 6, adopting $T_{\text{rot}} = 10$ or 13 K as mentioned above. Upper limits were estimated with the same approach as described for the CCS lines, with an average linewidth of the NH₃(1,1) main component of 0.85 km s^{-1} . This optical thin approximation has also been applied for sources which were detected, but for which no column density was derived in the papers of L96 and BHR95b. Note that for CB 230 and CB 232 the NH₃ measurement positions of L96 are offset by about one beam from the submillimeter cores detected by L2010 (identical to the CCS measurement position), and hence N_{NH_3} can be expected to underestimate the column density towards the cores.

For the calculation of the column densities given in Table 2 the beam filling factors f_b were adopted in the following way: for sources included in L96 and BHR95b the source sizes derived there were used to calculate the beam filling factor to be applied to our Parkes CCS measurements, assuming that CCS and ammonia emission have comparable spatial extents (which is an approximation, see e.g. Codella & Scappini 1998a). For the other sources, we used the average source sizes from the papers of L96 and BHR95b to calculate an average beam filling factor of $f_b = 0.81$ for the BHR, and 0.69 for the CB objects.

5. Discussion

5.1. Column densities and fractional abundances

The column densities of CCS and NH₃, shown in Table 2, do not exhibit strong dependence on the evolutionary group of the corresponding source, although the highest values for N_{CCS} are found for group 0 objects. Column densities of NH₃ versus those of CCS are displayed in Fig. 2 (without the omitted sources mentioned in Sect. 4). The lower right part of the plot is occupied exclusively by sources undetected in CCS (i.e. only upper limits for N_{CCS}); all sources with $N_{\text{NH}_3} < 1.5 \times 10^{14} \text{ cm}^{-2}$ have ammonia column densities obtained with the optical thin approximation. Sources with reliable detection of both molecules are found preferentially in the upper left side of the plot, as if the highest CCS column densities are present (or excited) only in globules with high ammonia column density, while lower values of N_{CCS} can be found in objects with a wider range of N_{NH_3} .

However, no clear distinction is visible between the distribution of the presumably younger objects of group –I and the actively star-forming globules (groups 0 and I).

The large scatter of the column densities likely results from differences in the hydrogen densities of the individual clouds, therefore a comparison of fractional abundances is required for a reasonable discussion of possible evolutionary trends. Hydrogen column densities or masses for several globules were derived from dust emission by L2010, from C¹⁸O measurements by L96, Wang et al. (1995) and Vilas-Boas et al. (1994), and from extinction by Racca et al. (2009). Some globules of our sample are included simultaneously in three of these studies; for these the column densities N_{H} of L2010 (derived by dividing the hydrogen masses from their work by the proton mass and the physical area enclosed by the 1.3 mm dust emission in the maps) and L96 are found to be systematically larger than those of Wang et al. (1995) by a factor of 7.6 and 2 (within 20%), respectively. Thus, we assume the same conversion factors for the rest of the globules in the according works to bring them on the scale of Wang et al. (1995), but we do not use this approach for Racca et al. (2009) and Vilas-Boas et al. (1994) since there is an overlap of only one source with the other studies. For 15 globules with reliable evolutionary stage this yields fractional abundances $N_{\text{CCS}}/N_{\text{H}}$ of 7×10^{-11} to 6×10^{-10} and $N_{\text{NH}_3}/N_{\text{H}}$ between 2×10^{-9} and 1×10^{-7} . For CCS, the fractional abundance averaged over globules of the same evolutionary group is very similar for group –I, 0 and I (about 3×10^{-10}). For NH₃ it is highest for group 0 (6×10^{-8}) and lowest for group I (1×10^{-8}), but this variation should not be considered significant due to the large scatter between individual globules and their small number. These estimated fractional abundances are comparable with those of several chemical models from the literature and an own model, which will be described later in Sect. 5.2, at evolutionary times close to 10^5 yrs. Comparing with the fractional abundances observed for dense cores in cloud complexes from Foster et al. (2009), $N_{\text{NH}_3}/N_{\text{H}}$ from the globules is similar, but $N_{\text{CCS}}/N_{\text{H}}$ is about one order of magnitude lower than in the dense cores. However, as pointed out earlier in this section, the hydrogen column densities of the globules vary up to one order of magnitude between different studies and therefore the fractional abundances of CCS and NH₃ estimated here have to be considered uncertain to the same degree.

5.2. NH₃/CCS ratio in comparison with chemical models

In contrast, the relative abundance $N_{\text{NH}_3}/N_{\text{CCS}}$ can be discussed independent of the hydrogen densities under the assumption that both molecules trace similar cloud regions, which is likely because of comparable excitation conditions and a similar telescope beam for both observations. Figure 3 shows $N_{\text{NH}_3}/N_{\text{CCS}}$ versus evolutionary group. Altogether, we derive abundance ratios from about 20 to 860, while the observable range is limited to ca. $N_{\text{NH}_3}/N_{\text{CCS}} \leq 2000$ by our CCS detection limit.

Compared to samples of earlier papers, the $N_{\text{NH}_3}/N_{\text{CCS}}$ ratios derived for isolated Bok globules are on average similar to those of dense cores in the Perseus molecular cloud (Rosolowsky et al. 2008), but a factor of two higher than those in the dark clouds studied by Suzuki et al. (1992). This corresponds to the fact that despite a comparable range of ammonia column densities in the Suzuki et al. (1992) sample and our globules, we do not find extremely high CCS column densities typical of carbon-chain producing regions (e.g. Hirota et al. 2009, where carbon-chain producing regions are defined as having $N_{\text{NH}_3}/N_{\text{CCS}} \leq 10$).

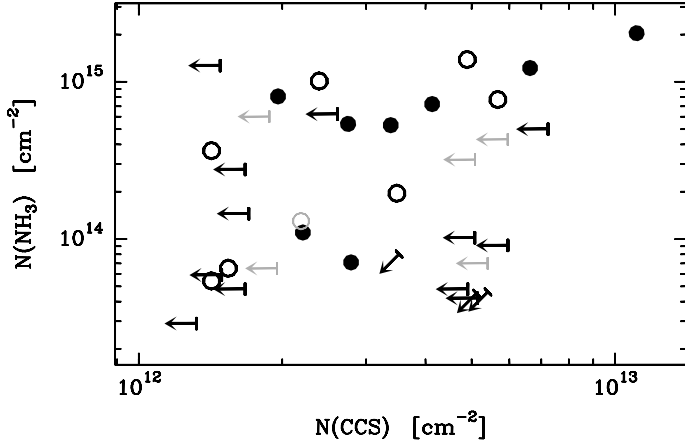


Fig. 2. Column densities of NH₃ versus CCS. Arrows indicate upper limits; filled and open circles represent objects with evidence for ongoing star formation (group 0 and I) and no signs of current star formation (group –I), respectively. Grey symbols denote sources with uncertain evolutionary group (given in brackets in Table 2).

The number of sources is too small to allow for a detailed statistical analysis, but taking into account only sources with reliable evolutionary stage, the following picture arises: within each evolutionary group, a relatively large range of abundance ratios $N_{\text{NH}_3}/N_{\text{CCS}}$ spanning about one order of magnitude is observed, but there is comparatively little variation of the values between the different groups. Fig. 3 possibly suggests a slightly decreasing tendency of $N_{\text{NH}_3}/N_{\text{CCS}}$ going from group 0 to group I globules, but this trend is only marginal. Thus, it can be concluded that the ratio $N_{\text{NH}_3}/N_{\text{CCS}}$ is rather similar across the Bok globules observed in this study, despite them harbouring YSOs in different evolutionary stages.

Specifically, the $N_{\text{NH}_3}/N_{\text{CCS}}$ ratio does not increase going from the presumably youngest objects of group –I to the most evolved sources of group I. This finding does not easily fit into the general picture of most chemical models, according to which CCS as an early-phase molecule is expected to decrease in abundance rapidly around 10^6 yr, while the slowly forming ammonia reaches its maximum abundance in a later stage of the chemical evolution – leading to the anticipation of steadily increasing $N_{\text{NH}_3}/N_{\text{CCS}}$ ratio along with the evolutionary stage of the globules. For comparison, we show in Fig. 4 the $N_{\text{NH}_3}/N_{\text{CCS}}$ ratio with respect to the chemical age of a cloud, calculated from the evolution of CCS and NH₃ abundances from four chemical models in the literature: Suzuki et al. (1992, dash-dotted line) and Scappini et al. (1998, dashed line) use pseudo-time-dependent chemical models in which the gas density is constant within time. In contrast, Bergin (2000, solid line) and Aikawa et al. (2001, dotted line) take into account the dynamics of a collapsing core, as well as depletion of species from the gas phase onto, and desorption from, dust grains. However, both models do not include reactions on grain surfaces except of H₂ formation and ion-electron recombination in Aikawa et al. (2001). As initial conditions all models take hydrogen in molecular form and carbon and sulphur as ions, the initial abundances are taken as those typical of diffuse clouds or depleted by a certain factor from solar abundances; Bergin (2000) allow the cloud to evolve for 1.5×10^5 yr at constant density and take the chemical composition after this time as initial values for the dynamically evolving core. All models consider the chemical evolution in a region at a constant temperature of 10 K and shielded from external UV

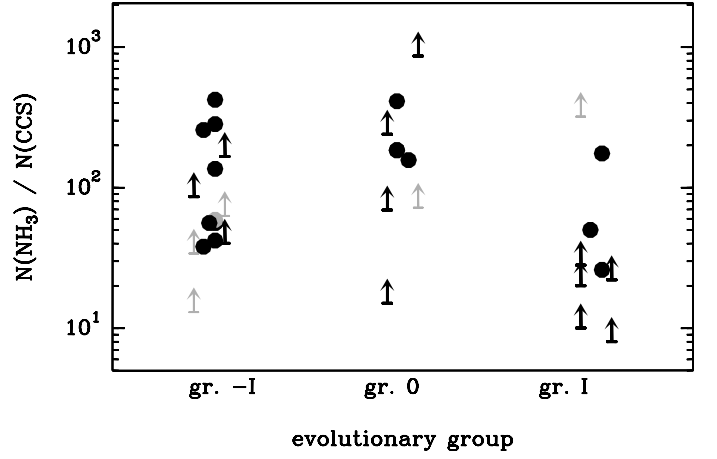


Fig. 3. Abundance ratio $N_{\text{NH}_3}/N_{\text{CCS}}$ versus evolutionary group; arrows indicate lower limits and grey symbols sources with uncertain evolutionary group (slight horizontal offsets around the group positions are solely for better visibility of individual data-points).

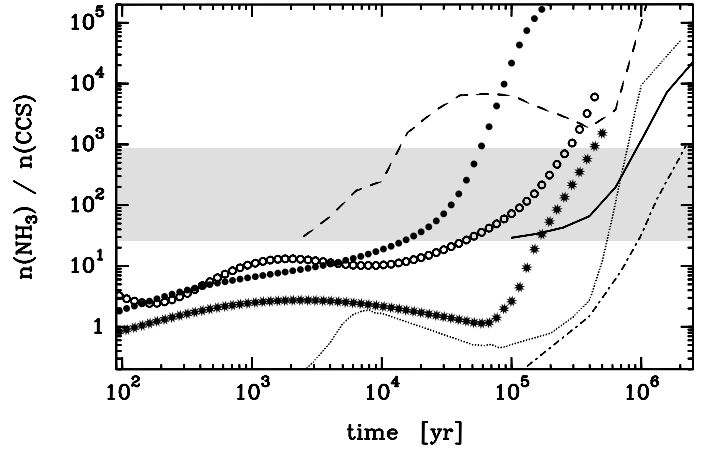


Fig. 4. NH₃/CCS ratio from chemical model calculations (see Sect. 5.2) of Suzuki et al. (1992, dash-dotted line), Scappini et al. (1998, dashed line), Bergin (2000, solid line) and Aikawa et al. (2001, dotted line), and this work (10 K warm group –I model marked with open circles, 15 K group 0 model with filled circles and 25 K group I model with asterisks). The observed range of $N_{\text{NH}_3}/N_{\text{CCS}}$ is designated by the shaded area.

radiation. Aikawa et al. (2001) follow the chemical evolution of an infalling fluid element in a collapse according to the Larson-Penston solution (we show here their result for a collapse slowed down by a factor of 10). From Bergin (2000) we show the model for a collapse with ambipolar diffusion and dust grains covered with a CO mantle. Both papers examine several variations of their models (e.g. grain properties, collapse timescales), which result in somewhat different time evolutions of the molecular abundances, but do not deviate significantly from the examples shown in Fig. 4.

Despite the different approaches, all models agree upon a rapid increase of the $N_{\text{NH}_3}/N_{\text{CCS}}$ ratio by three orders of magnitude at an evolutionary time of several 10^5 yr, caused by a fast decrease of the CCS abundance due to depletion onto grains, destruction by reactions and missing replenishment. The first broad peak seen in the results of Scappini et al. (1998) and Aikawa et al. (2001) is due to a very slow formation and in-

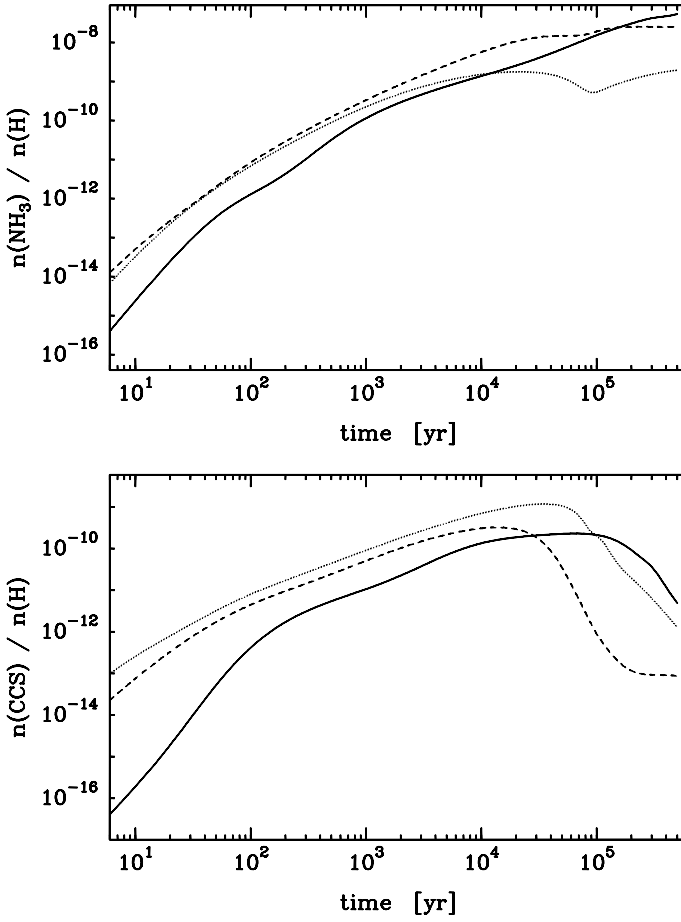


Fig. 5. Upper part: Evolution of the NH₃ fractional abundance resulting from our model described in Sect. 5.2 for group –I model (10 K, solid line), group 0 model (15 K, dashed line) and group I model (25 K, dotted line). Lower part: The same for CCS.

crease of the NH₃ abundance, while CCS is still being formed efficiently.

In general, a comparison of the absolute values observed with those from modelling has to be considered with caution. The initial conditions assumed and the exact starting point for reactions defined in chemical models might not necessarily be in good agreement with real globules, and certain scatter has to be expected due to the natural fluctuations of initial conditions in the variety of globules. Nevertheless, comparing the measured values for $N_{\text{NH}_3}/N_{\text{CCS}}$ abundance ratio with the models suggests that the observed objects might all be in an evolved state matching the region after 10⁵ yr despite their different evolutionary stages. In addition, we employed an own chemical

model to calculate abundances of NH₃ and CCS for sources of the three groups –I, 0 and I. For this purpose a recent chemical network including a variety of grain surface reactions (Semenov et al. 2010) was used together with a simplified physical model. Representative physical parameters for each group were taken from the globule study by L2010, i.e. the density is described by a power law function of radius (with exponent between –1 and –2) in the outer region and flattening towards the core center. We used a temperature of 10 K for group –I, 15 K for group 0, and 25 K for group I sources, respectively, based on observations and models of the mass-averaged dust temperature (L2010 and references therein). Starting from “low metal”

atomic abundances (Lee et al. 1998) as initial values, the evolution of NH₃ and CCS abundance relative to H was calculated separately for the typical physical conditions of each group. We refrained from constructing a piecewise model with sharp transitions from one group to the next at defined timesteps, since in reality a smooth transition of physical conditions can be expected, and the lifetimes of the different groups are not tightly constrained. Instead, we discuss qualitative differences of the three models.

The resulting evolution of fractional NH₃ and CCS abundances is displayed in Fig. 5. In our chemical model, CCS forms fast in a neutral-neutral reaction of CCH and S, and reaches its maximum concentration early. NH₃ is formed partly on dust grains through surface hydrogenation of nitrogen, and partly in the gas phase mainly via a sequence of ion-molecule reactions. Desorption from grain surfaces occurs mainly through cosmic-ray heating and cosmic-ray-induced far-UV photons in the cold and shielded environments considered here. After a few 10⁵ yrs CCS is efficiently removed from the gas phase by freeze out onto dust grains or destruction by reactions with oxygen, and rapidly drops in abundance. For the 15 and 25 K warm group 0 and group I models, prior to this late-time depletion of CCS a number of competitive surface reactions become active, which enhance the CCS (re)production and lower the NH₃ abundance, resulting in a temporary drop of the NH₃ abundance at about 10⁵ yrs and a slightly increased CCS peak abundance compared to the 10 K model of group –I sources. For other carbon-chain molecules, a similar enhancement in moderately warm environments (“warm carbon-chain chemistry”) has been pointed out recently (e.g. Sakai et al. 2008; Aikawa et al. 2008; Hassel et al. 2008). These differences in chemical evolution of our models originate primarily from the different temperatures, while the difference in density profiles has smaller influence. For simplicity, we will refer to the models of the three groups (–I, 0 and I) by their temperature (10, 15 and 25 K) in the following.

As a result, in the early phase the ratio $N_{\text{NH}_3}/N_{\text{CCS}}$ evolves very slowly from values close to unity to few dozen for all three models. For the 10 K model, the abundance ratio starts to increase faster around 10⁵ yrs and crosses the range observed in the Bok globules of our sample within 2.5×10^5 yrs. For the somewhat warmer 15 K model, $N_{\text{NH}_3}/N_{\text{CCS}}$ increases earlier and more rapidly, while for the 25 K model the abundance ratio remains low (< 10) until $> 1 \times 10^5$ yrs before increasing rapidly to $> 10^3$ like the other two models. In Fig. 4, the evolution of $N_{\text{NH}_3}/N_{\text{CCS}}$ for the three parameter sets of our chemical model is designated by open and filled circles (10 K and 15 K, respectively) and asterisks (25 K).

Comparing with the observational data shown in Fig. 3, the observed range of $N_{\text{NH}_3}/N_{\text{CCS}}$ ratios could be compatible with the rapidly increasing parts of our three model curves at evolutionary times of few 10⁴–10⁵ yrs. However, the 10 K and 15 K model are close to the lower $N_{\text{NH}_3}/N_{\text{CCS}}$ limit derived from our observations for most of their evolutionary time, while the 25 K model remains at significantly lower values up to 10⁵ yrs. Thus, if one assumes that the actual chemical ages of Bok globules may possess a certain scatter, one could also expect to find globules with very low $N_{\text{NH}_3}/N_{\text{CCS}}$ ratios (≤ 5) if the group I model is applicable – but such low ratios are not confirmed in our sample. The range of fractional abundances estimated from the observations in Sect. 5.1 agrees for NH₃ with both 10 and 15 K model for times $> 10^4$ yrs, while the NH₃ abundance in the 25 K model remains slightly below the observed range for the whole time span covered by the model. For CCS, the peak abundances of 10 and 15 K model around 10⁴–10⁵ yrs fall into the observed range,

while the 25 K model exceeds it. Although having to keep in mind the uncertainties of the estimated fractional abundances, this may be another indication that the 25 K model is not in agreement with the observations, while 10 and 15 K warm model fit them equally well.

Originally, the choice of 10–25 K for the models of the different groups was motivated by models (e.g., Shirley et al. 2002; Galli et al. 2002; Bergin et al. 2006) and observations (e.g. for CB 244 in Stutz et al. 2010) of the dust temperature. In general, dust temperatures are expected to be elevated (~ 15 K) close to the cloud surface heated by the interstellar radiation field, and lower (~ 10 K) in the moderately dense envelope where CO line radiation cools the gas efficiently. In the center of prestellar cores they may be as low as 5 K (depending on the external radiation field), or accordingly warmer in the case of an internal heating source (20–30 K in Shirley et al. 2002). In the dense ($n_{\text{H}} \geq 10^5 \text{ cm}^{-3}$) inner regions gas and dust are expected to be well coupled through collisions and hence similar in temperature.

In contrast, the beam- (BHR95b) or map-averaged (L96) NH₃ rotational temperatures (which represent a good estimate of the kinetic temperature at the low temperatures prevalent in globules, see e.g. Stutzki 1984) are 9–16 K for globules of all evolutionary stages (L96; BHR95b). This most likely results from the fact that the warm cores of Class 0 and more evolved objects have typical sizes of few thousand AU (L2010), and hence comprise only a small fraction of the NH₃ beam area for the average globule distance of our sample. In addition, the innermost warmest and densest parts of the core may not be traced well by NH₃ due to high optical depth. Thus, with the large beam of the NH₃ observations considered here, cool (~ 10 –15 K) gas from the moderately dense envelope can be expected to dominate the signal (see also Crapsi et al. 2007, where the central gas temperature drop in a prestellar core is detectable with interferometric, but not single-dish observations).

Moreover, a scatter of temperatures in the range 10–15 K for the bulk of gas may also result from differences in size, density and local UV background radiation for the individual globules, and not only from their evolutionary stage. In Foster et al. (2009) the kinetic temperatures from NH₃ of protostellar and starless cores cover a similar range as those for our globules, and the slight differences between the star-forming and starless group detected by them may be discernable only for sample sizes significantly larger than ours.

If indeed, as suggested by our chemical model, small temperature differences of ~ 5 K could already perceptibly affect the progression of the $N_{\text{NH}_3}/N_{\text{CCS}}$ ratio around 10^5 yrs, then the superposition of $N_{\text{NH}_3}/N_{\text{CCS}}$ evolution curves for several initial temperatures could lead to a relatively large scatter of $N_{\text{NH}_3}/N_{\text{CCS}}$ ratios within one evolutionary group, while simultaneously smearing out differences between the evolutionary groups (differences of other initial physical parameters as density may also contribute, but we do not address them here in detail since the observational data is too sparse for comparison). This would agree with the observation that the (beam-averaged) $N_{\text{NH}_3}/N_{\text{CCS}}$ ratio is rather similar across globules of all evolutionary stages and exhibits a relatively large scatter within each group. Additional contributions to the scatter of the $N_{\text{NH}_3}/N_{\text{CCS}}$ abundance ratio among globules of a single group may arise from the significant fraction of globules containing adjacent objects of different evolutionary stages (Sect. 2), indicative of sequential star formation, and a range of ages even among the objects compiled in one evolutionary group.

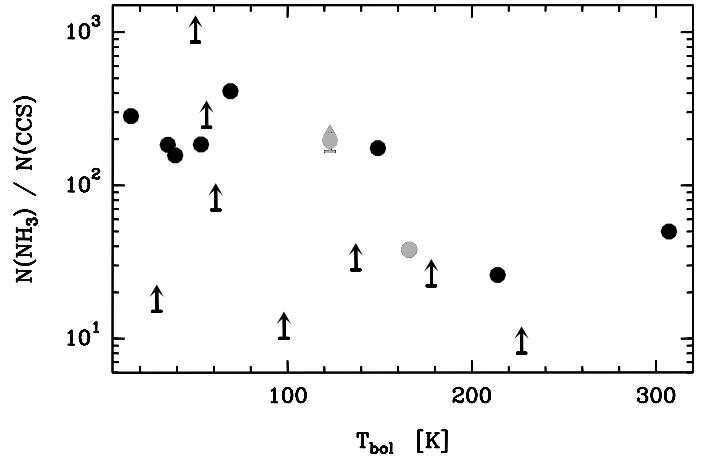


Fig. 6. Abundance ratio $N_{\text{NH}_3}/N_{\text{CCS}}$ versus bolometric temperature of embedded sources. Arrows indicate lower limits of the abundance ratio, grey symbols mark T_{bol} of combined spectral energy distributions (cf. Sect. 5.3).

To test this hypothesis in detail, it would be necessary to disentangle the influence of gas temperature and age (i.e. evolutionary group), for which our dataset is significantly too small. It could also be of interest to evaluate a possible increase of gas temperature and change of chemistry on small scales close to forming protostars, for which observations at much higher resolution are needed.

5.3. Abundance ratio and bolometric temperature

In the previous years it has been pointed out that the evolution of young stellar objects is well traced by the bolometric temperature T_{bol} , defined as the temperature of a blackbody with the same mean frequency as the spectrum of the observed source (Ladd et al. 1991; Myers & Ladd 1993). Chen et al. (1995) demonstrated a tight correlation between T_{bol} and the age of protostars and pre-main-sequence stars in particular for embedded sources. For a number of young stellar objects in globules of our sample, the bolometric temperature has been evaluated by L2010 and Racca et al. (2009). However, T_{bol} is mainly useful to track the evolution of Class 0 and later sources, since for most of the coldest, presumably youngest sources (e.g. CB 246, BHR 137) T_{bol} is not known due to a spectral energy distribution not well constrained at shorter wavelengths.

We show our measured $N_{\text{NH}_3}/N_{\text{CCS}}$ abundance ratio versus T_{bol} adopted from the works by L2010 and Racca et al. (2009), in Fig. 6. In the case of CB 232 and CB 243 (as well as BHR 12 denoted in grey colour), where both a prestellar core and a Class I source are included in the beam, T_{bol} represents the value for the combined spectral energy distribution of the adjacent sources, which is in both cases dominated by the Class I source while the molecular emission is expected to emerge mainly from the prestellar cores. However, in both globules the separation of prestellar core and Class I source equals the typical size of a prestellar core (8000 AU in L2010); in this case the presence of an evolved YSO might influence the chemistry of the prestellar core and accordingly both may be not completely unrelated. For a definite judgement about this question, a mapping of the line emission at small scales would be required.

From most chemical models in the literature as shown in Fig. 4, an increase of the $N_{\text{NH}_3}/N_{\text{CCS}}$ ratio towards warmer bolometric temperatures, which in turn are thought to represent in-

creasingly older and more evolved sources, would be expected. Despite the scarceness of our dataset, there are no indications of such an increase. Instead, the $N_{\text{NH}_3}/N_{\text{CCS}}$ abundance ratio shows a tentatively trend of decrease towards increasing bolometric temperature. However, due to the small number of globules with both known bolometric temperature and detected CCS emission, an interpretation is even more difficult than in Sect. 5.2.

5.4. Nonthermal linewidths

The observed linewidths Δv_{obs} include an instrumental broadening of $\Delta v_{\text{instr}} = 0.08 \text{ km s}^{-1}$ (Effelsberg) and 0.05 km s^{-1} (Parkes) which can be subtracted under the assumption of a Gaussian profile for the line as well as for the spectrometer:

$$\Delta v^2 = \Delta v_{\text{obs}}^2 - \Delta v_{\text{instr}}^2 \quad (8)$$

In the same way, the thermal contribution to the linewidth,

$$\Delta v_{\text{therm}} = \sqrt{\frac{8 \ln 2 k T_{\text{kin}}}{m}} \quad (9)$$

with m denoting the molecular mass of the molecule, was subtracted to obtain the nonthermal linewidths Δv_{nth} in Table 2. We used the rotational temperature T_{rot} derived by L96 and BHR95b from their ammonia observations as an estimate for the kinetic temperature T_{kin} . Where such values for the individual globules were not available, an average temperature of $T_{\text{kin}} = 10 \text{ K}$ was assumed. The typical thermal contribution for the CCS and NH₃ linewidths is 0.09 and 0.16 km s^{-1} , respectively. It should be pointed out that, because the main component of the NH₃(1,1) line consists of several usually blended hyperfine components distributed over 0.7 km s^{-1} , linewidths derived from a single Gaussian fit to the main component are dominated by the separation of the blended hyperfine components rather than the intrinsic linewidth for small linewidths. An intrinsic linewidth can be in principle estimated from such fits, but suffers from large uncertainties for the typical small linewidths observed in Bok globules. Therefore we discuss nonthermal linewidths of only those globules with sufficiently well detected main and satellite lines of NH₃(1,1), for which intrinsic linewidths can be derived directly from fits of the hyperfine structure.

For both NH₃ and CCS, the majority of nonthermal linewidths is found in the range $0.2\text{--}0.5 \text{ km s}^{-1}$ for all evolutionary groups. In addition, large nonthermal linewidths $0.6\text{--}1.2 \text{ km s}^{-1}$ are observed in globules of group 0 and I, while very small linewidths $\leq 0.1 \text{ km s}^{-1}$ are present exclusively in globules of group -I. The nonthermal linewidth can be understood as a measure for turbulence of the medium and the existence of unresolved velocity components within the area covered by the telescope beam. An increased linewidth Δv_{nth} for actively star-forming regions could be expected due to turbulence and outflow motions induced by the presence of a protostar. However, for globules at larger distances a physical region of proportionally larger dimension is enclosed by the beam, and could therefore result in larger linewidths. We are fairly confident that our results are not biased by this effect, since no clear relationship between linewidth and distance is discernable in our sample.

Among the starless or prestellar sources of group -I, the globules with extremely small nonthermal linewidths (CB 22 and CB 23) are distinguished from the rest by an absence of IRAS and millimeter sources, i.e. there is no evidence for any embedded sources. In contrast, three of the group -I globules with intermediate Δv_{nth} harbour more evolved Class I sources

in the vicinity of the prestellar core, while the remaining globules are poorly studied. The group 0 and I sources with large nonthermal linewidths exhibit not very Gaussian-shaped profiles (BHR 140-1, BHR 36) or hints of at least two velocity components (BHR 71, also BHR 55). However, they do not differ distinctly from the rest of the group 0 and I globules in properties like presence of outflows, multiplicity, etc.

In the majority of globules, the nonthermal CCS linewidths are smaller than those of NH₃, but also the opposite case or similar linewidths are observed. A possible explanation could be that both molecules trace not exactly similar cloud regions, as in the cases demonstrated by Codella & Scappini (1998b) and Lai & Crutcher (2000), where the most dense parts of cores were preferentially detected in NH₃, while CCS emission arises from a more extended surrounding region. Such central depletion holes in evolved sources have also been observed for other carbon-bearing species, e.g. for the CCH radical (e.g., Beuther et al. 2008; Padovani et al. 2009), which resembles in many properties, and is thought to be a precursor of, CCS. Since both NH₃ and CCS possess a roughly comparable critical density ($\sim 10^3\text{--}10^4 \text{ cm}^{-3}$), a difference in the emitting region is most likely a result of different spatial distributions.

This in turn might mean that both molecules trace regions with somewhat different physical conditions, and also result in an incorrect estimate of the thermal component for the linewidths when assuming the same kinetic temperature for both CCS and NH₃. Altogether, it is difficult to draw firm conclusions regarding the origin of the spread of nonthermal linewidths due to the sparse dataset and availability of only single-point measurements.

6. Summary

Observations of 42 Bok globules in CCS and partially in NH₃, supplemented with NH₃ measurements from the literature (L96, BHR95b) enabled us to assess the abundance ratio of both molecules for 18 objects (and derive lower limits for additional 21 globules) in different evolutionary stages ranging from starless and prestellar globules (designated as group -I) over clouds containing Class 0 YSOs (group 0) to globules harbouring young stellar objects of Class I and later (group I). In the following we summarize our main results:

1. The CCS(2₁-1₀) line is detected in 18 of 42 Bok globules. The detection rate is highest in the objects of group -I (70%) and decreases towards the globules of group 0 and I (40 and 33%, respectively). Ammonia is detected (together with literature data) in 39 globules.
2. We derive $N_{\text{NH}_3}/N_{\text{CCS}}$ ratios in the range 26–422, plus one lower limit of 860, for isolated Bok globules. In particular, within the limits of our survey, we find neither extremely low abundance ratios (≤ 10) like those typical of carbon-chain producing regions in dark cloud (Suzuki et al. 1992; Hirota et al. 2009), nor extremely high abundance ratios (several 10^3) as expected for evolved sources from chemical models for cloud cores by different authors (Fig. 4).
3. We do not observe an increase of the $N_{\text{NH}_3}/N_{\text{CCS}}$ abundance ratio going from the starless and prestellar globules towards evolved globules containing Class I or later sources, nor from lower towards higher bolometric temperatures of the embedded YSOs, as would be expected from various chemical models from the literature and this work (Sect. 5.2). Instead, the ratio exhibits a considerable scatter but is roughly con-

stant across all evolutionary groups (Fig. 3), with a tentatively - however, statistically not significant - decreasing trend from globules containing Class 0 protostars (group 0) towards globules with Class I or later YSOs (group I).

4. An own chemical model (Sect. 5.2) indicates that a slight temperature increase (15 instead of 10 K) could affect the $N_{\text{NH}_3}/N_{\text{CCS}}$ ratio perceptibly at evolutionary times around 10^5 yrs. Since NH₃ rotational temperatures vary in the same range, this may suggest that the observed roughly constant but scattered distribution of (beam-averaged) $N_{\text{NH}_3}/N_{\text{CCS}}$ ratios could result from a superposition of evolutionary tracks for different initial globule temperatures. In contrast, a 25 K warm model seems less likely, since neither such high gas temperatures, NH₃ and CCS fractional abundances in agreement with the model, nor very low $N_{\text{NH}_3}/N_{\text{CCS}}$ ratios (≤ 5), as expected from the model even at late evolutionary times, are observed.
5. The smallest nonthermal linewidths of CCS ($\sim 0.1 \text{ km s}^{-1}$), indicating a very low level of turbulence, are detected only in two globules of group -I without any associated infrared or millimeter sources. In contrast, broad CCS lines with evidence for multiple velocity components are found only among star-forming globules (groups 0 and I). Beyond that, no firm conclusions about the nonthermal linewidths can be drawn due to the small sample size.

We conclude that our observed $N_{\text{NH}_3}/N_{\text{CCS}}$ abundance ratios derived from single-dish observations with relatively large beam, although related to the evolutionary state of the embedded objects, cannot be alone and straightforward interpreted as an evolutionary tracer for isolated Bok globules. Another major problem hampering this study is the immediate vicinity of objects in different evolutionary stages encountered in many of the globules (see also L2010), which makes it difficult to assess the amount of emission arising from each source or a possible mutual influence on physical and chemical conditions. In addition, the assumption of NH₃ and CCS tracing the same spatial regions is an approximation and may not hold for all globules. The distribution of CCS – central depletion hole or enhanced in the warm core region of evolved sources – is of particular interest. Well-resolved mapping of the line emission of both molecules for a large sample of globules, assessment of the gas temperature, and a position-dependent evaluation of the $N_{\text{NH}_3}/N_{\text{CCS}}$ ratio, will be required to address the mentioned aspects in full detail.

Acknowledgements. We would like to express our thanks to the staff of the Effelsberg 100-m telescope and the Parkes 64-m telescope for their assistance with the observations. M. Ilgner contributed with helpful discussions. C.M. acknowledges support from the Deutsche Forschungsgemeinschaft (DFG) through grant SCHR665/7-1 during part of this study. We thank an anonymous referee and M. Walmsley for valuable comments and suggestions which helped to improve this paper.

References

- Aikawa, Y., Ohashi, N., Inutsuka, S., Herbst, E., & Takakuwa, S. 2001, *ApJ*, 552, 639
- Aikawa, Y., Wakelam, V., Garrod, R. T., & Herbst, E. 2008, *ApJ*, 674, 984
- Alves, J. & Yun, J. 1994, in *Astronomical Society of the Pacific Conference Series*, Vol. 65, *Clouds, Cores, and Low Mass Stars*, ed. D. P. Clemens & R. Barvainis, 230–233
- Alves, J. F. & Yun, J. L. 1995, *ApJ*, 438, L107
- André, P., Ward-Thompson, D., & Barsony, M. 1993, *ApJ*, 406, 122
- Bergin, E. A. 2000, in *IAU Symposium*, Vol. 197, *From Molecular Clouds to Planetary*, ed. Y. C. Minh & E. F. van Dishoeck, 51
- Bergin, E. A., Maret, S., van der Tak, F. F. S., et al. 2006, *ApJ*, 645, 369
- Beuther, H., Semenov, D., Henning, T., & Linz, H. 2008, *ApJ*, 675, L33
- Bok, B. J. & Reilly, E. F. 1947, *ApJ*, 105, 255
- Bourke, T. L., Hyland, A. R., & Robinson, G. 1995a, *MNRAS*, 276, 1052
- Bourke, T. L., Hyland, A. R., Robinson, G., James, S. D., & Wright, C. M. 1995b, *MNRAS*, 276, 1067, (BHR95b)
- Chen, H., Myers, P. C., Ladd, E. F., & Wood, D. O. S. 1995, *ApJ*, 445, 377
- Clemens, D. P. & Barvainis, R. 1988, *ApJS*, 68, 257
- Clemens, D. P., Yun, J. L., & Heyer, M. H. 1991, *ApJS*, 75, 877
- Codella, C. & Bachiller, R. 1999, *A&A*, 350, 659
- Codella, C. & Scappini, F. 1998a, *MNRAS*, 298, 1092
- Codella, C. & Scappini, F. 1998b, *MNRAS*, 298, 1092
- Codella, C. & Scappini, F. 2003, *MNRAS*, 344, 1257
- Crapci, A., Caselli, P., Walmsley, M. C., & Tafalla, M. 2007, *A&A*, 470, 221
- de Gregorio-Monsalvo, I., Gómez, J. F., Suárez, O., et al. 2006, *ApJ*, 642, 319, (dGM06)
- Foster, J. B., Rosolowsky, E. W., Kauffmann, J., et al. 2009, *ApJ*, 696, 298
- Galli, D., Walmsley, M., & Gonçalves, J. 2002, *A&A*, 394, 275
- Hassel, G. E., Herbst, E., & Garrod, R. T. 2008, *ApJ*, 681, 1385
- Henning, T. & Launhardt, R. 1998, *A&A*, 338, 223
- Hirota, T., Ohishi, M., & Yamamoto, S. 2009, *ApJ*, 699, 585
- Ho, P. T. P. & Townes, C. H. 1983, *ARA&A*, 21, 239
- Huard, T. L., Sandell, G., & Weintraub, D. A. 1999, *ApJ*, 526, 833
- Huard, T. L., Weintraub, D. A., & Sandell, G. 2000, *A&A*, 362, 635
- Lada, C. J. 1987, in *IAU Symposium*, Vol. 115, *Star Forming Regions*, ed. M. Peimbert & J. Jugaku, 1–17
- Ladd, E. F., Adams, F. C., Casey, S., et al. 1991, *ApJ*, 366, 203
- Lai, S.-P. & Crutcher, R. M. 2000, *ApJS*, 128, 271
- Launhardt, R., Evans, II, N. J., Wang, Y., et al. 1998a, *ApJS*, 119, 59
- Launhardt, R. & Henning, T. 1997, *A&A*, 326, 329, (LH97)
- Launhardt, R., Henning, T., & Klein, R. 1998b, in *Astronomical Society of the Pacific Conference Series*, Vol. 132, *Star Formation with the Infrared Space Observatory*, ed. J. Yun & L. Liseau, 119–125
- Launhardt, R., Nutter, D., Ward-Thompson, D., et al. 2010, *ApJS*, 188, 139, (L2010)
- Lee, C. W. & Myers, P. C. 1999, *ApJS*, 123, 233
- Lee, C. W., Myers, P. C., & Plume, R. 2004, *ApJS*, 153, 523
- Lee, C. W., Myers, P. C., & Tafalla, M. 1999, *ApJ*, 526, 788
- Lee, H., Roueff, E., Pineau des Forets, G., et al. 1998, *A&A*, 334, 1047
- Lemme, C., Wilson, T. L., Tieftrunk, A. R., & Henkel, C. 1996, *A&A*, 312, 585, (L96)
- Moreira, M. C. & Yun, J. L. 1995, *ApJ*, 454, 850
- Moreira, M. C., Yun, J. L., Torrelles, J. M., Afonso, J. M., & Santos, C. A. 1999, *AJ*, 118, 1315
- Moreira, M. C., Yun, J. L., Vazquez, R., & Torrelles, J. M. 1997, *AJ*, 113, 1371
- Myers, P. C. & Ladd, E. F. 1993, *ApJ*, 413, L47
- Otrupcek, R. E., Hartley, M., & Wang, J. 2000, *PASA*, 17, 92
- Padovani, M., Walmsley, C. M., Tafalla, M., Galli, D., & Müller, H. S. P. 2009, *A&A*, 505, 1199
- Petrie, S. 1996, *MNRAS*, 281, 666
- Racca, G. A., Vilas-Boas, J. W. S., & de la Reza, R. 2009, *ApJ*, 703, 1444
- Rosolowsky, E. W., Pineda, J. E., Foster, J. B., et al. 2008, *ApJS*, 175, 509
- Sahu, M. & Sahu, K. C. 1992, *A&A*, 259, 265
- Saito, S., Kawaguchi, K., Yamamoto, S., et al. 1987, *ApJ*, 317, L115
- Sakai, N., Ikeda, M., Morita, M., et al. 2007, *ApJ*, 663, 1174
- Sakai, N., Sakai, T., Hirota, T., & Yamamoto, S. 2008, *ApJ*, 672, 371
- Santos, N. C., Yun, J. L., Santos, C. A., & Marreiros, R. G. 1998, *AJ*, 116, 1376
- Scappini, F., Caselli, P., & Palumbo, G. G. C. 1991, *MNRAS*, 249, 763
- Scappini, F., Cecchi-Pestellini, C., Olberg, M., Casolari, A., & Fanti, C. 1998, *ApJ*, 504, 866
- Scappini, F. & Codella, C. 1996, *MNRAS*, 282, 587
- Semenov, D., Hersant, F., Wakelam, V., et al. 2010, *A&A*, 522, 42
- Shirley, Y. L., Evans, II, N. J., & Rawlings, J. M. C. 2002, *ApJ*, 575, 337
- Stutz, A., Launhardt, R., Linz, H., et al. 2010, *A&A*, 518, L87+
- Stutzki, J. 1984, PhD thesis, Universität Köln
- Suzuki, H., Yamamoto, S., Ohishi, M., et al. 1992, *ApJ*, 392, 551
- Ungerechts, H., Walmsley, C. M., & Winnewisser, G. 1980, *A&A*, 88, 259
- Urquhart, J. S., Morgan, L. K., & Thompson, M. A. 2009, *A&A*, 497, 789
- van Dishoeck, E. F. & Blake, G. A. 1998, *ARA&A*, 36, 317
- Vilas-Boas, J. W. S., Myers, P. C., & Fuller, G. A. 1994, *ApJ*, 433, 96
- Walsh, A. J., Hyland, A. R., Robinson, G., & Burton, M. G. 1997, *MNRAS*, 291, 261
- Wang, Y., Evans, II, N. J., Zhou, S., & Clemens, D. P. 1995, *ApJ*, 454, 217
- Wolkovitch, D., Langer, W. D., Goldsmith, P. F., & Heyer, M. 1997, *ApJ*, 477, 241
- Yun, J. L. & Clemens, D. P. 1992, *ApJ*, 385, L21
- Yun, J. L. & Clemens, D. P. 1994a, *AJ*, 108, 612
- Yun, J. L. & Clemens, D. P. 1994b, *ApJS*, 92, 145
- Yun, J. L. & Clemens, D. P. 1995, *AJ*, 109, 742